CCRL2 Expression by Specialized Lung Capillary Endothelial Cells Controls NK-cell Homing in Lung Cancer

Francesca Sozio[1], Tiziana Schioppa[2,3], Mattia Laffranchi[1], Valentina Salvi[2], Nicola Tamassia[4], Francisco M. Bianchetto-Aguilera[4], Laura Tiberio[2], Raffaella Bonecchi[3,5], Daniela Bosisio[2], Marc Parmentier[6], Barbara Bottazzi[3], Roberto Leone[3], Eleonora Russo[1], Giovanni Bernardini[1], Stefano Garofalo[7], Cristina Limatola[7,8], Angela Gismondi[1], Giuseppe Sciumè[1], Alberto Mantovani[3,5,9], Annalisa Del Prete[2,3], and Silvano Sozzani[1,8]

ABSTRACT

Patterns of receptors for chemotactic factors regulate the homing of leukocytes to tissues. Here we report that the CCRL2/chemerin/CMKLR1 axis represents a selective pathway for the homing of natural killer (NK) cells to the lung. C–C motif chemokine receptor-like 2 (CCRL2) is a nonsignaling seven-transmembrane domain receptor able to control lung tumor growth. CCRL2 constitutive or conditional endothelial cell targeted ablation, or deletion of its ligand chemerin, were found to promote tumor progression in a $Kras/p53^{Flox}$ lung cancer cell model. This phenotype was dependent on the reduced recruitment of $CD27^-$ $CD11b^+$ mature NK cells. Other chemotactic receptors identified in lung-infiltrating NK cells by single-cell

RNA sequencing (scRNA-seq), such as Cxcr3, Cx3cr1, and S1pr5, were found to be dispensable in the regulation of NK-cell infiltration of the lung and lung tumor growth. scRNA-seq identified CCRL2 as the hallmark of general alveolar lung capillary endothelial cells. CCRL2 expression was epigenetically regulated in lung endothelium and it was upregulated by the demethylating agent 5-aza-2′-deoxycytidine (5-Aza). *In vivo* administration of low doses of 5-Aza induced CCRL2 upregulation, increased recruitment of NK cells, and reduced lung tumor growth. These results identify CCRL2 as an NK-cell lung homing molecule that has the potential to be exploited to promote NK cell–mediated lung immune surveillance.

Introduction

Leukocyte recruitment across specialized vascular endothelium is a process that characterizes both physiologic and pathologic conditions (1, 2). Chemotactic receptors and adhesion molecules are the two major classes of molecules responsible for the selective, organ-specific homing of leukocytes (3). In the presence of circulatory flow, glycosaminoglycans present on the luminal side of vascular endothelial cells are also required to retain chemokines locally and facilitate their interaction with circulating cells (4).

Chemotactic receptors are seven-transmembrane domain receptors that activate a complex G protein–dependent signaling cascade leading

to cell migration and activation (5). In addition to "classical" chemotactic receptors, chemotactic factors also bind to atypical chemokine receptors (ACKR), a subset of receptors unable to activate G proteins or to induce chemotaxis. This class of receptors can regulate local inflammation and immune response through chemokine scavenging, chemokine transcytosis, and by shaping the chemotactic gradient (5).

C–C motif chemokine receptor-like 2 (CCRL2) is a molecule closely related to CC chemokine receptors that, similarly to ACKRs, lacks the ability to signal through G proteins. However, differently from ACKRs, CCRL2 binds a nonchemokine chemotactic protein, chemerin, and does not activate β-arrestin–dependent signaling (6–8). Consequently, CCRL2 does not undergo high-rate internalization or promote ligand scavenging from extracellular fluids (6, 9), rather it functions as a molecule that immobilizes and possibly concentrates the ligand on the surface of CCRL2-expressing cells, such as endothelial cells (10, 11). This process is functional to promote β1-integrin–dependent arrest and adhesion (11) of circulating leukocytes expressing CMKLR1 (recently renamed $chemerin_1$; ref. 12), the signaling chemerin receptor, such as in the case of monocytes, dendritic cells (DC), and natural killer (NK) cells (13, 14).

Lung endothelial cells constitute a thin barrier with specialized functions in the exchange of gas between air and blood and are located at the site of leukocyte extravasation. The heterogeneity of mouse and lung endothelial cells was recently unraveled by single-cell transcriptome analysis (15, 16).

We have previously reported that the expression of CCRL2 protects mice in both genetic and chemically induced experimental models of lung tumors. This action was based on the nonredundant role of CCRL2 in the recruitment of NK cells to the lung and in the orchestration of antitumor immune surveillance (17). Here, we report that the role of CCRL2 in NK-cell orchestration of antitumor response is a peculiar trait of the lung. By combining genetic and transcriptional approaches and integrative single-cell RNA sequencing (scRNA-seq)

[1]Department of Molecular Medicine, Sapienza University of Rome, Laboratory Affiliated to Institute Pasteur-Italia, Rome, Italy. [2]Department of Molecular and Translational Medicine, University of Brescia, Brescia, Italy. [3]IRCCS Humanitas Research Hospital, Rozzano, Milan, Italy. [4]Department of Medicine, Section of General Pathology, University of Verona, Italy. [5]Department of Biomedical Sciences, Humanitas University, Pieve Emanuele, Milan, Italy. [6]WELBIO and I.R.I.B.H.M., Université Libre de Bruxelles, Brussels, Belgium. [7]Department of Physiology and Pharmacology, Sapienza University of Rome, Rome, Italy. [8]IRCCS Neuromed, Pozzilli (IS), Italy. [9]The William Harvey Research Institute, Queen Mary University of London, London, United Kingdom.

F. Sozio, T. Schioppa, and M. Laffranchi are the co–first authors of this article.

A. Del Prete and S. Sozzani are the co–last authors of this article.

Corresponding Author: Silvano Sozzani, Department of Molecular Medicine, Sapienza University of Rome, Viale Regina Elena 291, Rome 00161, Italy. Phone: 3906-4925-5115; E-mail: silvano.sozzani@uniroma1.it

analysis, we report that the confined expression of CCRL2 to a subset of specialized lung microvascular capillary endothelial cells selectively regulates NK-cell migration to the lung. Therefore, the CCRL2/chemerin/CMKLR1 axis represents a previously underappreciated pathway for the homing of NK cells to this organ.

Materials and Methods

Animals

Procedures involving animal handling and care were conducted according to protocols approved by the Humanitas Clinical and Research Center (Rozzano, Milan, Italy) in compliance with national (D.L. N.116, G.U., suppl. 40, 18–2-1992 and N. 26, G.U. March 4, 2014) and international laws and policies (EEC Council Directive 2010/63/EU, OJ L 276/33, 22–09–2010; NIH Guide for the Care and Use of Laboratory Animals, U.S. National Research Council, 2011). The study was approved by the Italian Ministry of Health (approval number 35/2013-B, issued on February 7, 2017 and number 165/2017-PR, issued on February 20, 2017). All efforts were made to minimize the number of animals used and their suffering. All female and male mice used are listed as follows: wild-type (WT), *Ccrl2* knockout (KO; ref. 18), TK *Ccrl2* WT, TK *Ccrl2* KO (17), *Cxcr3* KO (G. Bernardini, Sapienza University, Rome, Italy), *Cx3cr1* KO (C. Limatola, Sapienza University, Rome, Italy), *Chemerin* KO (M. Parmentier, ULB Medical School, Brussels, Belgium), *Cdh5*[Cre/ERT2];*Ccrl2*[f/f], *Cdh5*[Cre/ERT2];*Ackr2*[f/f], obtained by crossing *Cdh5*[Cre/ERT2] mice (kindly provided by Prof. Condorelli, Humanitas University, Milan, Italy) with *Ccrl2*[f/f] (recently obtained by S. Sozzani) and *Ackr2*[f/f] (Prof. Bonecchi Humanitas University, Milan, Italy), and *Cmklr1* KO (11)]. All mice were on a C57BL/6J genetic background and were 8 to 12 weeks old, unless otherwise specified. All colonies were housed and bred in the Humanitas IRCCS SPF animal facility in individually ventilated cages, with the exception of *Cxcr3* KO and *Cx3cr1* KO mice, which were housed in the Sapienza University animal facility, and *Chemerin* KO mice, housed in the ULB Medical School Animal Facility, Bruxelles Belgium. To conditionally delete *Ccrl2* from vascular endothelium, *Cdh5*[Cre/ERT2];*Ccrl2*[f/f] mice were fed for 2 weeks with tamoxifen diet TAM400/CreER (TD.55125.I, Envigo) followed by one wash-out week before inoculation of tumor cell lines. *Cdh5*[Cre/ERT2];*Ackr2*[f/f] mice received tamoxifen diet to delete *Ackr2* from vascular endothelium. Genotyping of mice was performed by PCR.

Cell lines

The LUAD cell line KP10.21 was derived in our laboratory (January 2021) from primary lung tumors of C57BL/6J TK mice (*Kras*[G12D/+];*p53*[LoxP] mice) 10 weeks after intranasal administration of Ad5-CMV-Cre (AdenoCre ref. 17). The cell line was maintained in DMEM (Thermo Fisher Scientific) supplemented with 10% FBS and gentamicin (50 mg/mL; catalog no. G1397, Merck) and routinely tested for *Mycoplasma* contamination. KP10.21 cells were expanded to passage 3 and stored in aliquots in liquid nitrogen; to induce tumors, cells were cultured less than five passages before being inoculated into mice. The KP10.21 cell line was authenticated for the presence of the *Kras*[G12D]-mutated allele and *p53* gene deletion by PCR (*Kras*[G12D] primers: common reverse 5′-ctgcatagtacgctataccctgt-3′; wt forward 5′-tgtctttccccagcacagt-3′; mut forward 5′-gcaggtcgagggacctaata-3′; *p53* primers: forward 5′-ggttaaacccagctt-gacca-3′; reverse 5′-ggaggcagagacagttggag-3′; Supplementary Fig. S1). The Lewis Lung carcinoma (LLC) cell line was maintained in DMEM supplemented with 10% FBS and routinely tested for *Mycoplasma* contamination.

The mouse lung capillary endothelial cell line (1G11) was grown in complete medium [DMEM, 20% FBS, 1% nonessential amino acids (catalog no. M7145, Merck), 1 mmol/L sodium pyruvate (catalog no. S8636, Merck), 100 U/mL penicillin and streptomycin, freshly added heparin (catalog no. H3149), and endothelial cell growth supplement at final concentration of 100 µg/mL (catalog no. E2759, Merck)], as previously described (11). 1G11 cells were grown to confluence on 0.1% gelatin-coated 6-well plates and stimulated for 4 hours with the combination of mouse IFNγ (50 ng/mL, catalog no. 315–05, PeproTech), mouse TNFα (20 ng/mL. catalog no. 315–01A, PeproTech), and LPS (100 ng/mL, catalog no. L4005, Merck), or the combination of IFNγ and LPS in DMEM after 48-hour treatment with or without 5-aza-2′-deoxycytidine (5-Aza, 1 µmol/L, catalog no. A3656, Merck).

Tumor models and *in vivo* treatments

To establish lung orthotopic tumors, 1×10^5 KP10.21 cells in 100 µL PBS were injected intravenously in different mouse strains. For LLC cells, 5×10^5 cells in 100 µL PBS were injected intravenously in WT and *Ccrl2* KO mice. Lungs were collected 15 days after engraftment to perform histology and flow cytometric analysis. For the subcutaneous model, 5×10^5 KP10.21 cells in 100 µL PBS were injected in the right flank. Tumor growth was measured with a digital caliper [$V = \frac{1}{2}$ (length × width^2)] from day 7 postinjection until day 15 when mice were sacrificed, and tumors harvested and processed for flow cytometric analysis.

For FTY720 treatment, mice were intraperitoneally injected with 1 mg/kg FTY720 (catalog no. SML0700, Merck) daily from day 0 to day 9. On day 15 postinjection, mice were sacrificed and lungs were collected for histology and flow cytometric analysis. For 5-Aza treatment, mice were intraperitoneally injected with 0.5 mg/kg 5-Aza every other day from day 0 to day 15 postinjection. On day 15, mice were sacrificed and lungs were collected for histology and flow cytometric analysis. For adoptive transfer experiments, NK cells were purified from the spleen of WT or *Cmklr1* KO mice by using an NK Negative Isolation Kit (catalog no. 130–115–818, Miltenyi Biotec) according to the manufacturer's instructions. A total of 1×10^6 NK cells were fluorescently labeled with 1 µmol/L of carboxyfluorescein succinimidyl ester (CFSE) and intravenously injected in WT and *Ccrl2* KO mice at day +14 after the injection of KP10.21 cells. After 24 hours, mice were sacrificed, and tumors harvested and processed for flow cytometric analysis.

Sample processing for flow cytometric analysis and histology

Mice were sacrificed and lungs and tumors harvested. Briefly, lungs were collected following intracardiac perfusion with cold PBS. Right lung lobes were mechanically cut into small pieces and then enzymatically treated with collagenase D (IV type, *Clostridium histolyticum*, catalog no. C5138, Merck) at 0.1 mg/mL and DNase I (from bovine pancreas grade 2, catalog no. 10104159001, Roche) at 0.02 mg/mL at 37°C for 30 minutes. The enzymatic reactions were stopped by EDTA (Sigma), and a single-cell suspension was obtained by filtering through a 70-µm cell strainer before staining for cytofluorimetric analysis. Left lung lobes were formalin fixed for 24 hours, dehydrated, and paraffin embedded for histologic analysis. Subcutaneous injected tumors were collected, weighed, and mechanically cut into small pieces before enzymatic digestion with collagenase D at 1 mg/mL and DNase at 0.02 mg/mL at 37°C for 30 minutes. The enzymatic reactions were stopped by EDTA (Sigma), and a single-cell suspension was obtained by filtering through a 70-µm cell strainer before staining for cytofluorimetric analysis.

Flow cytometry and FACS

Single-cell suspensions from lung and subcutaneous tumors were stained with the following antibodies: CD45-BV605 (clone: 30-F11, BD Biosciences) or –VioGreen (clone: REA737), NK1.1-PECF594 or -APC (clone: PK136, BD Biosciences), CCRL2-PE (clone BZ2E3, BD Biosciences), CD11b-FITC or PE-Vio770 (clone: REA592), CD27-PEVio615 (clone: REA499), CD4-Viobright615 or –PE-Vio770 or -ViobrightR720 (clone REA604), CD8-BV570 (clone 53–6.7, BioLegend) or -VioBlue or -PerCP or FITC (cloneREA601). CD49b-APC (clone REA541), CD49a-PE (clone: REA493), TCRβ-PerCPVio770 (clone: REA318), TCRγδ -VioBlue or -APCVio770 (clone: REA633), Ly6G-FITC (clone REA526), Ly6C-PE (clone 1G7.G10), CD19-VioBlue or-APCVio770 or -FITC (clone REA749), F4/80-PerCPVio770 OR -FITC (clone REA126), CD45RA-APC-Vio770 or PE-Vio770 (clone RA3–6B2), MHCII-FITC or –VioBlue (clone M5/114.15.2), SiglecH-PE or -FITC (clone REA819), CD11c-PerCPVio770 (clone: REA 754), CD3-PE or -APCVio770 or -PEVio770 (clone REA641), SiglecF-FITC (clone: REA798), CD31-APC (clone REA784), EpCam-VioBlue (clone REA977), CD127-PE (clone REA680), TCRβ FITC or PerCPVio770 (clone RA318), TCRγδ-APCVio770 or -VioBlue (clone REA633), NKp46-APC (clone REA815). Unless otherwise specified, the antibodies were from Miltenyi Biotec. Subsequently, cell viability was determined by Aqua LIVE/Dead-405 nm (L34965) or LIVE/Dead-633 nm (L10120) or LIVE/Dead-488 nm (L34969) staining according to the manufacturer's instructions (all Invitrogen). Sorting was performed using a FACSAria II (BD Biosciences) and flow cytometry was performed using a MACSQuant Analyzer 16 (Miltenyi Biotec). Data were analyzed with FlowJo software (Treestar). The authors adhered to the guidelines for the use of flow cytometry and cell sorting in immunologic studies (19).

Lung histology

Histology was performed on three formalin-fixed, paraffin-embedded (FFPE) longitudinal serial sections (150 μm apart, 4 μm in thickness) from each left lung, stained with hematoxylin and eosin (H&E, Merck), and scanned by VS120 Dot-Slide BX61 virtual slide microscope (Olympus Optical). The total area of lung lesions was obtained by manually tracing the perimeter of lesions using the Image Pro-Premiere 9.1.4 software (Media Cybernetics).

Lung immunofluorescence

Immunofluorescence (IF) staining for NKp46 and CD31 was performed on 4-μm FFPE lung sections (1 section/lung) rehydrated in alcohol (100%, 90%, 70%, and 50%; 1 minute each step) and placed in citrate buffer 1 mol/L (for 15 minutes in a Whirlpool microwave) for antigen retrieval. Unspecific binding sites were blocked for 30 minutes with Background sniper (catalog no. BS966, Biocare Medical). Samples were then incubated with primary antibodies goat anti-mouse NKp46 (catalog no. AF2225, R&D Systems) and Rat monoclonal anti-mouse CD31 (clone SZ31, DIA-310, DIANOVA) followed by donkey anti-goat 488 (catalog no. A-11055, Thermo Fisher Scientific) and donkey anti-rat 594 (catalog no. A-11007, Thermo Fisher Scientific) secondary antibodies. Matched IgG was used as a negative control (for NKp46, polyclonal goat IgG, catalog no. LS-C149359, LSBio; for CD31, Rat IgG2a, catalog no. 54447, Novus Biologicals). The total number of NK cells adhering to the vascular endothelium was evaluated on the entire sections under fluorescence microscope BX61 (Olympus Optical) using Image Pro-Premiere 9.1.4 software.

Gene expression analysis by qPCR

Lung and tumor tissue from WT and Ccrl2 KO mice were analyzed for mRNA expression of the indicated genes by qPCR. RNA was extracted with Qiazol (catalog no. 79306, Qiagen) according to the manufacturer's instructions and quantified by NanoDrop (Thermo Fisher Scientific). After RNA purification, reverse transcription was performed using 0.5 μg RNA, random hexamers and MMLV RT (catalog no. 28025013, Thermo Fisher Scientific). Gene-specific mouse primers used: Cxcl10 (forward: 5′-cgtcattttctgcctcatcctg-3′, reverse: 5′-ccgtcatcgatatggatgcagt-3′), Cx3cl1 (forward: 5′-catccgctat-cagctaaacca-3′, reverse: 5′-cagaagcgtctgtgctgtgt-3′), Ccl5 (forward: 5′-atacgcttccctgtcatcgct-3′, reverse: 5′-ggagatgccgatttttccca-3), Rarres2 (chemerin) (forward: 5′-ggagtgcacaatcaaaccaa-3′, reverse: 5′-ttttacc-cttggggtccatt-3′), Cxcl12 (forward: 5-ctgtgcccttcagattgttg-3′, reverse: 5′-taatttcgggtcaatgcaca-3′), Ccl2 (forward: 5′-agcatccacgtgttggctcagc-3′, reverse: 5′-cctctctcttgagcttggtgac-3′), Cxcl9 (forward: 5′-tctcgg-acttcactccaacaca-3′, reverse: 5′-actccacactgctccaggaaga-3′), Cxcl11 (forward: 5′-gaacaggaaggtcacagccatagc-3′, reverse: 5′-tcaactttgtcg-cagccgttactc-3′), Rpl32 (forward: 5′-gctgccatctgttttacggt-3′, reverse: 5′-tgactggtgcctgatgaact-3′).

The SsoAdvanced Universal SYBR Green Supermix (catalog no. 1725274, Bio-Rad Laboratories) for qPCR was used according to the manufacturer's instructions. Reactions were run in triplicates on a StepOne Plus Real-Time PCR System (Applied Biosystems) and the generated products analyzed by the StepOne Plus Software (version 2.3, Applied Biosystems). Gene expression was determined as relative expression to the housekeeping gene Rpl32 ($2^{-\Delta C_i}$).

Generation of scRNA-seq libraries

Live Lin$^-$CD45$^+$NKp46$^+$CD127$^+$ innate lymphoid cells (ILC) were sorted from lung suspensions derived from Kras$^{G12D/+}$;p53^{LoxP} WT and Ccrl2-deficient tumor-bearing mice ($n = 5$/group). A FACSAria II was used for cell sorting of indicated cell populations into PBS with 2 mmol/L EDTA and 1% FBS. Single-cell sequencing libraries were generated using BD Rhapsody Single-Cell Analysis system (BD Biosciences) according to the manufacture's protocol [BD Rhapsody Whole Transcriptome Analysis (WTA) catalog no. 665915 and 633801]. Two separate BD Rhapsody Cartridges (catalog no. 633733 and 633731, BD Biosciences) were used for the pooled WT and Ccrl2 KO samples. No custom indexes were used, and the resulting indexed libraries were pooled and paired-end sequencing was performed on an Illumina NextSeq 500, with a read length of 76-bp paired-end reads and a sequencing depth over 100^6 reads for samples. Sequence reads were aligned to the mouse reference genome\(GRCm38-PhiX-gencodevM19), following generation of barcode-gene matrices via the standard BD WTA Rhapsody analysis pipeline version 1.8 (BD Biosciences) on Seven Bridges (https://www.sevenbridges.com), following the manufacturer's recommendations. Data from ambient RNA was trimmed on the basis of nUMI number of unique molecular identifiers (nUMI)-barcode saturation curve.

scRNA cell clustering and differentially expressed gene profile of NK and ILC cells extracted from mice lung tumors

The R package Seurat v4.05 was used under RStudio v4.1.5 for data trimming, unsupervised clustering, and visualization according to the authors' guidelines (20).

In detail, to remove poor quality cells, doublets and stressed cells, we removed cells with a gene number less than 200, or higher than the 93th quantile. Mitochondrial gene ratio was calculated to filter out low-quality cells (mitochondrial ratio ≥ 10%). Because WT and Ccrl2 KO cells were processed in two different cartridges, we merged their

dataset with the Seurat "integration" function (21) and the resulting dataset was further processed with "SCTransform" for normalization and data scaling (22). Highly variable genes (HVG, $n = 3,000$) were also identified with the "SCTransform" function. The HVGs were used as input for principal component analysis (PCA). The first 30 PCAs were utilized in the subsequent analysis with a resolution of 0.25. With them, cells were then embedded by Uniform Manifold Approximation and Projection for Dimension Reduction (UMAP) plot. To assign cell identities, we applied the "FindAllMarkers" to identify differentially expressed genes (DEG) among all genes by using Wilcoxon rank sum test. We selected only genes that showed (i) a minimal expression (minimum pct $\geq 20\%$) in at least one cluster; (ii) an adjusted $P \leq 0.05$; (iii) an average log2-fold change (logFC) ≥ 0.2.

We identified cell contaminants (about 2% of the total cell number) that possessed markers typical of macrophages, B cells, and invariant NK T (iNKT) cells. In addition, one cluster of NK cells showed a strong enrichment of ribosomal and mitochondrial genes, suggesting that these were stressed cells. Therefore, these cells were removed from the analysis. Accordingly, we removed from the raw data of the contaminant cells and repeated the Seurat protocol.

For the definition of ILCs differentiation, dedicated immune signature module scores were added to each cell by the "AddModuleScore" function according to specific lists of known cell type markers derived from Robinette and colleagues (23).

scRNA cell clustering and DEG profile of lung mouse endothelial cells

Raw counts of mouse lung endothelial cells were downloaded from GSE (GSE160876, GSE165063, E-MTAB-7458). Data for mouse endothelial cells were obtained from the Droplet dataset of the "Tabula Muris Project" (24) and data for human endothelial cells were obtained from the "Tabula Sapiens Data Portal" (https://tabula-sapiens-portal.ds.czbiohub.org). Only the donors TSP1 and TSP2 were analyzed due to the very low number of lung endothelial cells present in the other donors.

All the datasets were processed with Seurat v4.05 as described above. We selected 3,000 HVGs, and the first 30 PCAs were utilized in the dimensional reduction, with a resolution of 0.3 for the mouse and 0.5 for the human datasets. To assign cell identities, we applied the "FindAllMarkers" as above, in addition to a dedicated lung endothelial cell gene signature derived from Gilich and colleagues (15).

Pseudotime analysis with Monocle3

Trajectory analysis of either our in-house ILC scRNA dataset or the built murine lung atlas, was performed using Monocle3 according to the authors' guidelines (25).

Gene ontology enrichment analysis

Gene Ontology (GO) analyses were performed using the "g:Profiler" web source (26) on the murine lung scRNA dataset. The dedicated marker genes per cluster or the DEGs were subjected to a functional enrichment analysis. The resulting P values were adjusted for multiple testing using Bonferroni, and the ones that exceeded the 0.05 P value threshold were listed in Supplementary Table S1. The data source queried were KEGG (https://www.genome.jp/kegg/), Reactome (https://reactome.org/), WikiPathways (https://www.wikipathways.org/index.php/WikiPathways), and CORUM (http://mips.helmholtz-muenchen.de/corum/).

Spatial transcriptomic analysis of human lung alveoli

Raw data of a Visium Spatial Gene Expression assay ($10\times$ Genomics) on human lungs (GSE178360, https://doi.org/10.1038/s41586-022-

04541-3) were analyzed using the Seurat standard pipeline. Briefly, the data were normalized using the function "SCTransform". Dimensional reduction was performed using the commands "RunPCA" and "RunUMAP" and the resulting gene markers per cluster were obtained with the function "FindAllMarkers", using as threshold: (i) a minimal expression (minimum pct $\geq 20\%$); (ii) an adjusted $P \leq 0.05$; (iii) an average $\log_2$ fold change (logFC) ≥ 0.2.

Analysis of the non–small cell lung cancer dataset from The Cancer Genome Atlas

Lung adenocarcinoma (LUAD) RNA-seq (as FPKM, fragments per kilobase of exon per million mapped fragments) and DNA Methylation Array data (as beta values) were downloaded from the The Cancer Genome Atlas/Genomic Data Commons (TCGA/GDC; DbGaP Study Accession: phs000178) with the R package "TCGAbiolinks" (v2.28.3). Only samples with both CCRL2 expression and methylation data were kept (total of 473, 21 Normal Tissue and 452 Primary Tumor). The data were than processed in R according to the TCGA guidelines. Briefly, for the RNA-seq data the obtained FPKM were normalized with the R package "edgeR" (v3.42.4) and "limma" (v3.56.2). In parallel, the methylation data were processed with the R package "edgeR", "limma", "DMRcate" (v2.14.0), "minfi" (v1.46.0) and "missMethyl" (v1.34.0). For visualization, the R packages "ggplot2" (v3.4.2), "corrplot" (v0.92) and "RcolorBrewer" (v1.1–3) were utilized.

Statistical analysis

Statistical analyses were performed by Student t test, Wilcoxon rank sum test, Mann–Whitney test, one-way and two-way ANOVA with Bonferroni correction as appropriate. Results were analyzed by using GraphPad Prism (v7.04) and R (v4.2.1) software and expressed as mean ± SEM (*, $P < 0.05$; **, $P < 0.01$; ***, $P < 0.001$).

Data and software availability

The novel scRNA-seq dataset originated with this paper is accessible in the Gene Expression Omnibus (GEO) database under the accession number GSE212088. All other data generated in this study are available within the article and its Supplementary Data files or from the corresponding authors upon reasonable request.

Results

CCRL2 plays a nonredundant role in NK-cell trafficking to the lung

In a previous study, CCRL2 was shown to control lung tumor growth in $Kras^{G12D/+};p53^{LoxP}$ mice (17). To further define the role of CCRL2 in tumor progression, a cell line (KP10.21) was generated from primary tumors that developed in $Kras^{G12D/+};p53^{LoxP}$ mice (17, 27). This cell line carries the parental $Kras^{G12D}$ mutation and p53 deletion (Supplementary Fig. S1A) and when inoculated intravenously it recapitulated the phenotype observed in $Kras^{G12D/+};p53^{LoxP}$ parental mice (17), with histologic analysis revealing a significant increase in the number of tumor lesions in lungs of Ccrl2-deficient mice compared with WT animals (**Fig. 1A**). Because this type of tumor is under the control of NK cells (17), lung NK-cell infiltration (evaluated as CD3⁻NK1.1⁺ among live CD45⁺ cells, see Supplementary Fig. S1B for gating strategy) was investigated in KP10.21 injected mice. As in the prior study (17), the exacerbated tumor phenotype observed in Ccrl2-deficient mice was associated with a reduction of lung-infiltrating NK cells, evaluated both as percentage and total number of cells (**Fig. 1B**). Results also show that NK-cell infiltration closely paralleled tumor growth with a slight effect at day +7 (low tumor growth with negligible
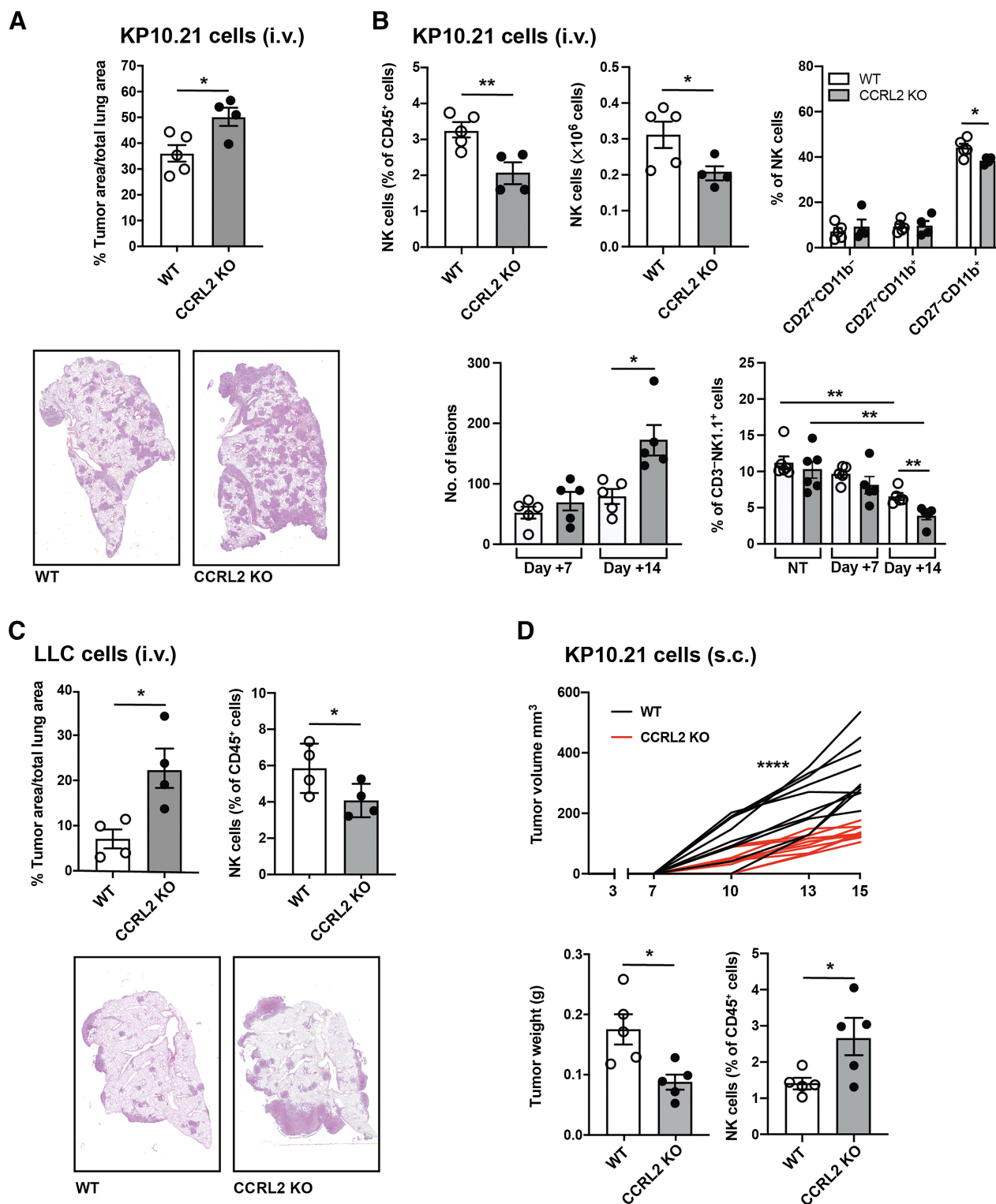
Figure 1.
Ccrl2 deficiency increases orthotopic (intravenous), but not heterotopic (subcutaneous), growth of lung tumor cell lines. **A,** Top, percentage of area occupied by tumor lesions on total lung sections of WT and *Ccrl2*-deficient (KO) mice intravenously injected with 1×10^5 KP10.21 cells and sacrificed 15 days later. *, $P < 0.05$, WT ($n = 5$) versus *Ccrl2* KO mice ($n = 4$) by Student t test. Bottom, representative images of H&E staining of WT and *Ccrl2* KO lungs; magnification, 10×. **B,** Top, flow cytometric analysis of NK cells, expressed as percentage and absolute number, in the CD45$^+$ population from mechanically and enzymatically treated WT and *Ccrl2* KO lungs. **, $P < 0.01$; *, $P < 0.05$, WT ($n = 5$) versus. *Ccrl2* KO mice ($n = 4$) by Student t test. (*Continued on the following page.*)

reduction of NK cells) and significant reduction of NK cells at day +14 (**Fig. 1B**). As previously observed in $Kras^{G12D/+};p53^{LoxP}$ mice (17), the decrease of NK cells was mostly related to the altered relative distribution of NK-cell subsets, with the most marked reduction in the more mature $CD27^-CD11b^+$ NK-cell subset (**Fig. 1B**). Independently of their relative frequency, NK cells showed similar distribution in WT and *Ccrl2*-deficient mice (17). A similar phenotype was observed in mice injected intravenously with LLC cells. As depicted in **Fig. 1C**, following LLC intravenous inoculation, an increased number of tumor foci and reduced infiltration of NK cells were detected in the lung of *Ccrl2*-deficient mice. In contrast, when KP10.21 cells were engrafted subcutaneously, *Ccrl2*-deficient mice were protected from tumor growth. This condition was associated with increased NK cell infiltration (**Fig. 1D**). We previously reported that *Ccrl2*-deficient mice were protected from tumor growth also when LLC cells were engrafted subcutaneously (28). qPCR analysis did not reveal any major differences in the expression of NK-cell chemotactic proteins (e.g., *Cxcl9, Cxcl10, Cxcl11, Cx3cl1, Ccl2,* and *Ccl5*) among the two genotypes and the different route of cancer cell inoculation. The only exception being *chemerin*, which showed a trend toward reduction in the lung of *Ccrl2*-deficient mice (Supplementary Fig. S1C). Collectively these results demonstrated that CCRL2 exerts different roles in controlling the expansion of tumor cells in relation to the site of tumor growth (i.e., lung vs. subcutaneous).

The possible role of chemotactic receptors known to be involved in NK-cell recruitment (i.e., CXCR3, CX3CR1, and S1PR5; refs. 29, 30) was investigated *in vivo*. **Figures 2A–C** show that among the three chemotactic receptors investigated only *Cxcr3* deficiency was associated with a partial reduction of total lung NK-cell recruitment; no effects were, otherwise, observed in *Cx3cr1*-deficient mice and in mice treated with the S1PR5 inhibitor FTY720. The individual block of each of the three receptors did not affect tumor growth or the relative distribution of lung NK-cell subsets (**Fig. 2A–C**).

Finally, the role of chemerin was investigated using *chemerin*-deficient mice. **Figure 2D** shows that in *chemerin*-deficient mice injected i.v. with KP10.21 cells, increased tumor growth was associated with reduced recruitment of NK cells, fully recapitulating the phenotype observed in *Ccrl2*-deficient mice. Similarly, NK-cell subset distribution revealed a decreased frequency of $CD27^-CD11b^+$ and an increase of the $CD27^+CD11b^-$ NK-cell subsets. Although multiple chemotactic factors are produced in the lung and several chemotactic receptors are potentially expressed by NK cells (31), collectively these results highlight the nonredundant role of CCRL2 for the *in vivo* trafficking of NK cells in response to lung cancer growth.

CCRL2 marks specialized lung endothelial cell subsets

Lung alveolar capillary endothelium represents the primary site of blood leukocyte trafficking to the lung (32) and CCRL2 is known to be expressed by endothelial cells (9, 10). To probe the distribution of CCRL2 among lung endothelial cell subsets, an atlas of mouse lung endothelium was assembled by integrating publicly available scRNA-seq datasets (33–35). Sixteen clusters were identified based on their enrichment with pulmonary endothelial gene signatures derived from Gillich and colleagues (15) (**Fig. 3A and B**; Supplementary Table S1). These included lymphatic, artery, vein, and alveolar capillary cells. Alveolar capillary endothelial cells can be divided into two molecularly defined subsets, aerocytes (aCaps), specialized in gas exchange, and general capillary cells (gCaps), involved in the regulation of vasomotor tone. Because of their location at the interface of blood with the external environment, lung endothelial cells are exposed to multiple challenges. Therefore, multiple clusters of gCaps and aCaps were resolved on the basis of their resting or activated (defined either as inflammatory or IFN-associated) gene profiles. In addition, clusters that were not positive for the considered gene signatures were collectively labelled as endothelial cells (**Fig. 3A and B**).

This analysis revealed that *Ccrl2* was a unique marker for the clusters gCap2 and inflammatory gCap, a subset of gCaps characterized by an NF-κB signature (**Fig. 3C**; Supplementary Fig. S2A; Supplementary Table S1). Consistent with the ability of IFNs to upregulate CCRL2 in endothelial cells (9–11), *Ccrl2* expression was also associated with clusters of both gCaps and aCaps carrying an IFN-signature (**Fig. 3C**; Supplementary Fig. S2A and Supplementary Table S1). Since gCaps can differentiate into aCaps (15), it could be possible that $CCRL2^+$ aCaps carrying an IFN-signature might originate from activated gCaps. However, pseudotemporal analysis did not support this hypothesis (Supplementary Fig. S2B). $Ccrl2^+$ gCap clusters coexpressed MHC class II molecules, a marker of gCaps (Supplementary Fig. S2A; Supplementary Table S1; ref. 15). This observation was confirmed at the protein level in our experimental conditions, using $CD31^+CCRL2^+$ cells purified from the lung of *Ccrl2* WT mice carrying the $Kras^{G12D/+};p53^{LoxP}$ mutation. Under basal conditions, MHC class II molecules were coexpressed with CCRL2 by a small subset of lung endothelial cells with the number of double positive cells strongly increasing during tumor growth (Supplementary Fig. S2C). The analysis of endothelial cells from the 12 organs deposited in the Tabula Muris project (24) confirmed that, among the different organs investigated, under homeostatic conditions, *Ccrl2* is selectively expressed by lung gCaps, with the only exception of kidney endothelial cells (Supplementary Fig. S2D). Collectively, these findings identify CCRL2 as a marker of specialized lung capillary endothelial cell subsets. The selective expression of CCRL2 by lung alveolar capillary cells may explain why NK-cell migration into subcutaneous tumors was not regulated in *Ccrl2*-deficient mice (**Fig. 1D**). Indeed, differently from lung $CD31^+$ endothelial cells (**Fig. 3C**; Supplementary Fig. S2C), $CD31^+$ cells from subcutaneous tumors did not express CCRL2 by flow cytometric analysis (Supplementary Fig. S2E). The selective expression of CCRL2 by lung gCaps was also investigated in humans. $CD31^+$ cells were collected from the Tabula Sapiens atlas (36), which hosts scRNA-seq datasets from 24 organs, including the lung (Supplementary Fig. S3A). aCap and gCaps were identified

---

(*Continued.*) Flow cytometric analysis of NK-cell subsets, $CD27^+CD11b^-$, $CD27^+CD11b^+$, $CD27^-CD11b^+$ evaluated in $CD3^-NK1.1^+$ gated cells from WT and *Ccrl2* KO lungs. *, $P < 0.05$, WT ($n = 5$) versus. *Ccrl2* KO ($n = 4$) by Student *t* test. Bottom, number of tumor lesions (left) and percentage of NK cells (right) at day+7 and day+14 postinjection of KP10.21 cells. NT, no tumor (control mice). **C,** Top, percentage of the area occupied by tumor lesions on total lung area of WT and *Ccrl2* KO mice intravenously (i.v.) injected with 5×10^5 LLC cells and sacrificed 15 days later. *, $P < 0.05$, WT ($n = 4$) versus *Ccrl2* KO mice ($n = 4$) by Student *t* test. Flow cytometric analysis of NK cells in the $CD45^+$ population from mechanically and enzymatically treated WT and *Ccrl2* KO lungs. *, $P < 0.05$, WT ($n = 4$) versus *Ccrl2* KO mice ($n = 4$) by Student *t* test. Bottom, representative images of H&E staining of WT and *Ccrl2* KO lungs; magnification, 10×. **D,** Top, tumor growth of WT and *Ccrl2* KO mice subcutaneously (s.c.) injected in the right flank with 5×10^5 KP10.21 cells. ****, $P < 0.0001$, WT ($n = 10$) versus *Ccrl2* KO mice ($n = 10$) by two-way ANOVA. Bottom, tumor weight (g) of WT and *Ccrl2* KO subcutaneously injected tumors sacrificed 15 days later; *, $P < 0.05$ WT ($n = 5$) versus *Ccrl2* KO mice ($n = 5$) by Student *t* test. Percentage of NK cells in the $CD45^+$ population of subcutaneously injected tumors. *, $P < 0.05$, WT ($n = 5$) versus *Ccrl2* KO mice ($n = 5$) by Student *t* test.
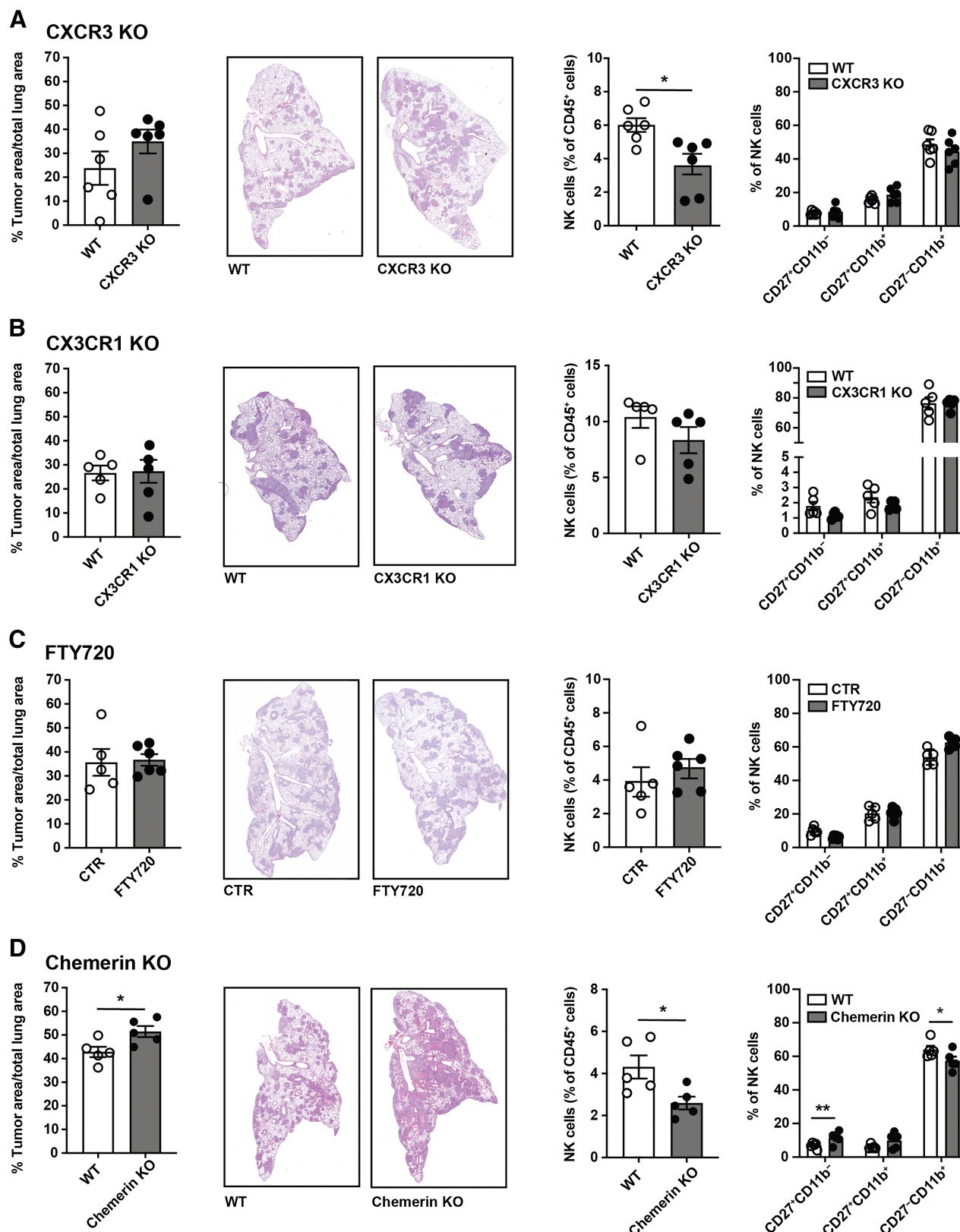
by their unique gene signatures (15) and specific enrichment in the lung (Supplementary Fig. S3B–S3C). Also in this dataset, *CCRL2* was selectively expressed by the gCap clusters (Supplementary Fig. S3D). This result was also confirmed in a lung spatial transcriptomic dataset (Supplementary Fig. S4; ref. 37). Together, these findings suggest that the selective expression of CCRL2 by lung alveolar endothelial cells is conserved in humans.

Immunohistologic analysis revealed that in *Ccrl2*-deficient mice fewer NK cells interact with CD31^{+} lung endothelial cells compared to WT animals, supporting a role for CCRL2 in NK-cell recruitment (**Fig. 3D**). To further investigate the functional relevance of CCRL2 expression by endothelial cells, *Ccrl2 flox/flox* (*Ccrl2^{f/f}*) mice were crossed with *Cdh5^{Cre/ERT2}* mice, which express the Cre recombinase under the control of a *Cdh5* promoter, to conditionally delete *Ccrl2* in vascular endothelium. Under these experimental conditions, the growth of KP10.21 lung tumor cells injected intravenously in *Cdh5^{Cre/ERT2}*;*Ccrl2^{f/f}* mice was increased with respect to control mice (**Fig. 3E**). In parallel, flow cytometric analysis showed a decreased frequency of lung-infiltrating NK cells. These results recapitulated the phenotype observed in constitutive *Ccrl2* deficient animals.

Finally, analysis of scRNA-seq datasets highlighted the expression of *Ackr2* by both aCap and gCap clusters expressing an IFN signature (**Fig. 3F**; Supplementary Table S1). ACKR2 is an atypical chemokine receptor previously reported to be involved in the regulation of leukocyte recruitment, including NK cells (38, 39). To evaluate the possible relevance of ACKR2 in lung NK-cell homing in our experimental conditions, KP10.21 tumor cells were injected i.v. in *Cdh5^{Cre/ERT2}*;*Ackr2^{f/f}* mice. **Figure 3G** shows that targeted deletion of ACKR2 in endothelial cells did not cause any alteration in either tumor growth or frequency of lung infiltrating NK cells. Therefore, these results do not support a role for ACKR2 expression by aCap and gCap in NK-cell homing to the lung.

scRNA analysis of NK cells and ILCs from lung tumors from WT and *Ccrl2*-deficient mice

In order to investigate whether lung NK cells express the biologically active chemotactic receptor for chemerin (CMKLR1), we profiled chemotactic receptors expressed by lung NK cells by scRNA-seq of total innate lymphocytes (**Fig. 4A**) purified from *Kras^{G12D/+}*;*p53^{LoxP}* (TK) WT and *Ccrl2*-deficient mice. A total of 12,980 cells were cataloged into eight distinct clusters (**Fig. 4B**). The distribution in

each cluster of the two genotypes was comparable (**Fig. 4C**; Supplementary Table S2). Clusters were identified as NK cells, ILC1, and ILC2 on the basis of their respective gene signatures (Supplementary Fig. S5A; Supplementary Table S2; ref. 23). The most abundant population was represented by NK cells distributed in six different clusters, with an overall distribution of 6,682 and 5,891 cells from WT and *Ccrl2*-deficient mice, respectively (Supplementary Table S2).

On the basis of their dedicated signatures, NK-cell clusters could be divided into two major populations. Five clusters were identified as mature NK cells (mNK1–5) based on expression of canonical markers, such as *Ly6c2, Malat1, Gzma, Irf8, Prf1*, and *Itgam* (CD11b; **Fig. 4D**; Supplementary Fig. S5B and Supplementary Table S2). Each of the mNK clusters was further distinguished on the basis of the unique expression of specific genes, such as *S1pr5* and *Klra8* (mNK1), *Ccl4* (mNK2), *Klra1* (mNK3), *Serpin9b* (mNK4), and *Hes1* (mNK5; **Fig. 4D**; Supplementary Fig. S5B and S5C and Supplementary Table S2). One single cluster showed the expression of marker genes associated with an early stage of NK-cell differentiation, such as *Ccr2, Tcf7, Emb*, and *Thy1*, and accordingly it was defined as immature NK cells (iNK; **Fig. 4D**; Supplementary Table S2). Although *Cd27* transcript was not captured by our scRNA-seq, other markers associated with an immature NK-cell phenotype (40), including *Nfkbia, Nr4a1*, and *Ccl4*, were highly expressed by the cells here defined as iNK cells. Thus, mature and immature clusters defined by scRNA-seq correspond to the NK-cell subsets identified by flow cytometric analysis in **Fig. 1B**.

On the basis of their unique molecular signatures, ILC1 and ILC2 cells were assigned to two dedicated clusters (**Fig. 4B** and **C**; Supplementary Fig. S5A). ILC2 were enriched in *Gata3, Il1rl1*, and *Il7r* (**Fig. 4D**; Supplementary Table S2) and represented a minute population, in agreement with their reported limited infiltration of the lung (41). In contrast, ILC1 were positive for canonical ILC genes, such as *Thy1, Rora, Cxcr6*, and *Tnfsf10* (**Fig. 4D**; Supplementary Table S2; ref. 42). These cells showed a noncytotoxic phenotype, being devoid of transcripts for granzymes (Supplementary Fig. S5B and S5D). The close proximity of the ILC1 and NK-cell clusters in the UMAP (**Fig. 4B**) supports the similarity of ILC1 and iNK clusters as further confirmed by pseudotemporal proximity analysis (ref. 43; Supplementary Fig. S6).

Analysis of molecules involved in NK-cell recruitment revealed the preferential expression of *S1pr5, Cx3cr1*, and *Cmklr1* in mNK cell

---

Figure 2.

CXCR3, CX3CR1, and S1PR5 are dispensable in orthotopic growth of KP10.21 cell line, while the CCRL2/chemerin/CMKLR1 axis is necessary. **A,** Left, percentage of area occupied by tumor lesions on total lung area of WT versus *Cxcr3* KO mice intravenously (i.v.) injected with 10^5 KP10.21 cells and sacrificed 15 days later. WT ($n = 6$) versus *Cxcr3* KO mice ($n = 6$) by Student t test. Representative images of H&E staining of WT and *Cxcr3* KO lungs. Magnification, 10×. Center, flow cytometric analysis of NK cells in the CD45^{+} population from mechanically and enzymatically treated WT and *Cxcr3* KO lungs. *, $P < 0.05$, WT ($n = 6$) versus *Cxcr3* KO mice ($n = 6$) by Student t test. Right, flow cytometric analysis of the main NK-cell subsets, CD27^{+}CD11b^{−}, CD27^{+}CD11b^{+}, CD27^{−}CD11b^{+} evaluated in CD3^{−}NK1.1^{+} gated cells from WT and *Cxcr3* KO lungs. **B,** Left, percentage of tumor lesions on total lung area of WT versus *Cx3cr1* KO mice intravenously injected with 10^5 KP10.21 cells and sacrificed 15 days later. WT ($n = 5$) versus *Cx3cr1* KO mice ($n = 5$). Representative images of H&E staining of WT versus *Cx3cr1* KO lungs. Magnification, 10×. Center, flow cytometric analysis of NK cells in the CD45^{+} population from mechanically and enzymatically WT versus *Cx3cr1* KO lungs. Right, FACS analysis of the main NK-cell subsets, CD27^{+}CD11b^{−}, CD27^{+}CD11b^{+}, CD27^{−}CD11b^{+} evaluated CD3^{−}NK1.1^{+} gated cells from WT versus *Cx3cr1* KO lungs. **C,** Left, percentage of tumor lesions on total lung area of FTY720- vs. PBS-treated (CTR) mice intravenously injected with 10^5 KP10.21 cells and sacrificed 15 days later. CTR ($n = 5$) versus FTY720-treated mice ($n = 6$). Representative images of H&E staining of CTR versus FTY720-treated lungs. Magnification, 10×. Center, FACS analysis of NK cells in the CD45^{+} population from mechanically and enzymatically treated CTR and FTY720-treated lungs. Right, flow cytometric analysis of the main NK-cell subsets, CD27^{+}CD11b^{−}, CD27^{+}CD11b^{+}, CD27^{−}CD11b^{+} evaluated CD3^{−}NK1.1^{+} gated cells from CTR and FTY720-treated lungs. **D,** Left, percentage of area occupied by tumor lesions on total lung area of WT and *Chemerin* KO mice intravenously injected with 10^5 KP10.21 cells and sacrificed 15 days later. *, $P < 0.05$, WT ($n = 5$) versus *Chemerin* KO mice ($n = 5$) by Student t test. Representative images of H&E staining of WT and *Chemerin* KO lungs. Magnification, 10×. Center, flow cytometric analysis of NK cells in the CD45^{+} population from mechanically and enzymatically treated WT and *Chemerin* KO lungs. *, $P < 0.05$, WT ($n = 5$) versus *Chemerin* KO mice ($n = 5$) by Student t test. Right, flow cytometric analysis of the main NK-cell subsets, CD27^{+}CD11b^{−}, CD27^{+}CD11b^{+}, CD27^{−}CD11b^{+} evaluated in CD3^{−}NK1.1^{+} gated cells from WT and *Chemerin* KO lungs. *, $P < 0.05$; **, $P < 0.01$, WT ($n = 5$) versus *Chemerin* KO ($n = 5$) by Student t test.
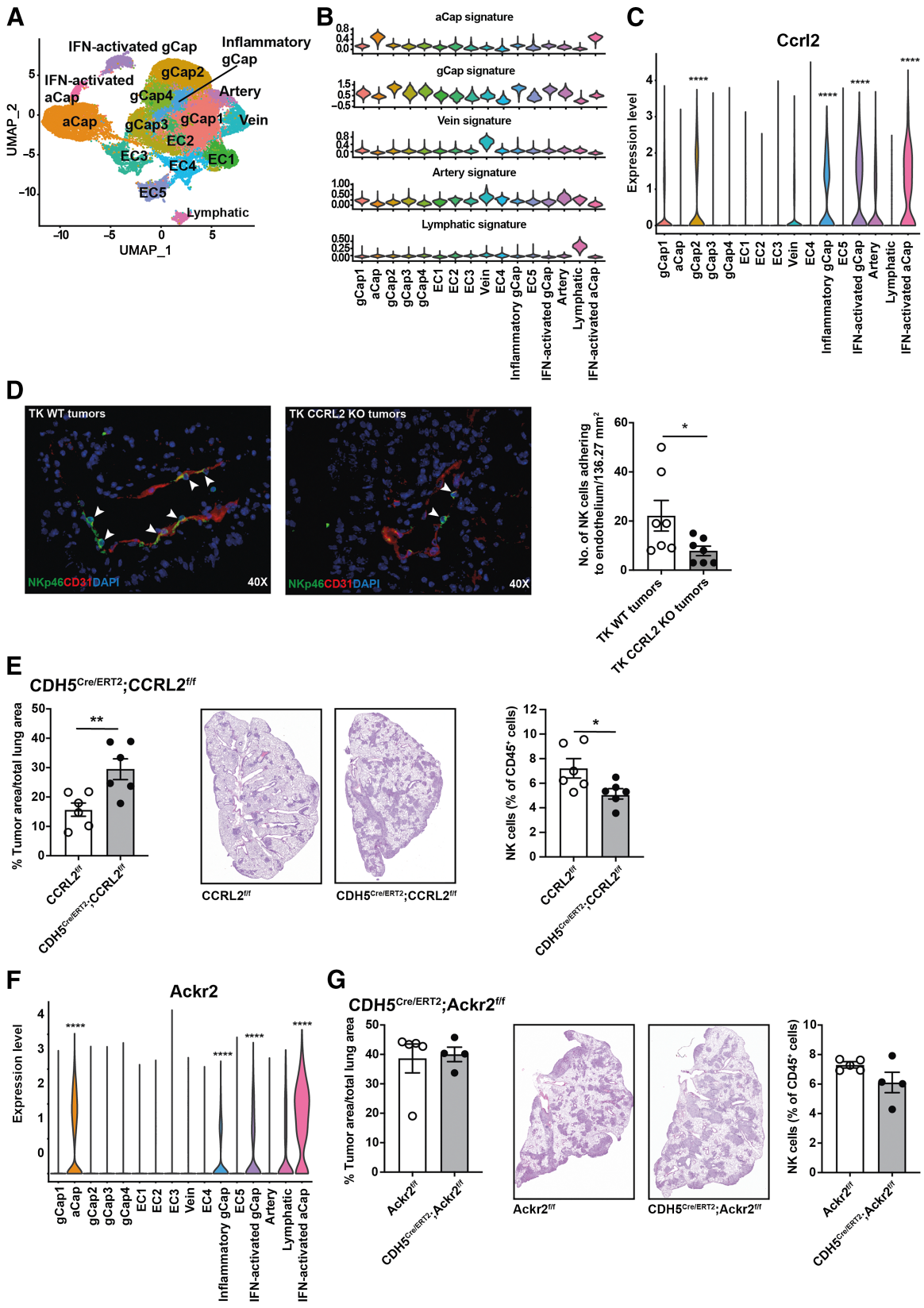
clusters (mNK1–5), while *Ccr2* and *Ccr5* were predominantly associated with iNK cells (**Fig. 4E**; Supplementary Table S2). These results are consistent with previously published reports (29). Among mNK cell clusters, *Cmklr1* was mostly expressed in cluster mNK4 together with several integrin α chains (*Itga1, Itga2, Itgam,* and *Itga4*) as well as integrin β chains (*Itgb1, Itgb2,* and *Itgb7*). Even though our scRNA-seq dataset was characterized by a generalized low capture of chemotactic receptor genes, *Cmklr1* and *Cx3cr1* appeared to colocalize in most of the mNK cell clusters. The pool of ILCs purified from *Ccrl2*-deficient mice contained fewer *Cmklr1*+ NK cells compared to WT mice, which is consistent with defective recruitment of *Cmklr1*+ NK cells in the absence of Ccrl2 (**Fig. 4F**). The role of CMKLR1 in NK-cell migration to the lung was further demonstrated by adoptive transfer experiments. NK cells purified from WT and *Cmklr1*-deficient mice were injected intravenously in WT and *Ccrl2*-deficient mice at day +14 after the injection of KP10.21 cells. Results, shown in **Fig. 4G**, depict a defect in the migration of *Cmklr1*-deficient cells to the lung. The magnitude of reduction observed was comparable with that observed in conditional endothelial cell targeted *Ccrl2*-deficient mice (**Fig. 3E**). The injection of NK cells into *Ccrl2*-deficient mice was strongly reduced independently of the genotype. This result suggests a cooperative role of CCRL2 with other chemotactic receptors in the homing to the lung.

CCRL2 expression is epigenetically regulated

We previously reported that in primary human lung adenocarcinoma (TCGA-LUAD), *CCRL2* gene expression positively correlated with clinical outcome (17). Because aberrant DNA methylation tends to accumulate during cancer progression, included LUAD (44), the same TCGA dataset was interrogated to investigate *CCRL2* methylation profile. **Figure 5A** shows that in primary tumor samples, *CCRL2* is hypermethylated and that the reduced expression of *CCRL2* in cancer tissue correlated with the increased methylation status of specific *CCRL2* genomic regions (**Fig. 5B**).

5-Aza is a demethylating drug approved for clinical use for the treatment of different cancers, including myelodysplastic syndrome, acute myeloid leukemia (AML), and lung cancer (45, 46). *In vitro* and *in vivo* administration of 5-Aza has been shown to promote leukocyte recruitment, including NK cells (47), through the regulation of various genes involved in cell migration, including proteases, chemokines, and chemokine receptors (48, 49). On the basis of these observations, the effect of 5-Aza on *Ccrl2* expression was evaluated using 1G11 cells, a mouse lung capillary endothelial cell line (9, 11), *in vitro*. **Figure 5C** shows that *Ccrl2* mRNA levels were increased when 1G11 cells were stimulated with proinflammatory signals. The effect of proinflammatory agonists was further increased in the presence of 5-Aza, suggesting

that CCRL2 expression is regulated by gene methylation. The possible therapeutic role of 5-Aza was tested in mice intravenously injected with KP10.21 lung tumor cells. Low doses of 5-Aza (0.5 mg/kg) were administered intraperitoneally every other day. **Figure 5D** shows that *in vivo* treatment with 5-Aza caused the upregulation of CCRL2 in lung endothelial cells both as percentage and MFI of positive cells. 5-Aza administration increase intratumoral infiltration with CD3+ cells, while other cell populations, such as CD8+ T cells and CD11b+Ly6G+ cells were not significantly affected by the treatment (Supplementary Fig. S7). The frequency of lung-infiltrating NK cells was also increased (**Fig. 5E**). The treatment with 5-Aza also caused a significant decrease in the number of tumor lesions as the possible result of combined effector mechanisms activated by the drug, including the increased recruitment of NK cells (**Fig. 5F**).

Discussion

Chemokines and other chemotactic factors control the migratory patterns of leukocytes in both physiologic and pathologic conditions (1). Here, using a *Kras/p53*^{Flox} mutated lung cancer model, we report that the CCRL2/chemerin/CMKLR1 axis represents a selective pathway for the recruitment of antitumor effector NK cells to the lung. Other chemotactic receptors, such as CXCR3, CX3CR1, and S1PR5, expressed by NK cells could potentially contribute to the recruitment of NK cells to the lung (29, 30). However, using complementary genetic models we demonstrated that NK-cell recruitment and lung tumor growth were impaired only when the expression of *Ccrl2* or its ligand *chemerin* were prevented, as observed in *Ccrl2*-deficient mice, *Cdh5*$^{Cre/ERT2}$;*Ccrl2*$^{f/f}$ mice, and *chemerin* deficient mice. Genetic deletion of *Cxcr3* or *Cx3cr1* and inactivation of S1PR5 by FTY720 administration, were not effective in controlling lung NK-cell recruitment and lung tumor growth. These results demonstrate a role for CCRL2 at the blood–endothelial cell interface in the recruitment of circulating CMKLR1+ NK cells to the lung.

Lung infiltration by mature NK cells was strictly dependent on CCRL2 expression, being reduced in all the experimental conditions in which CCRL2 expression and/or function were impaired, but not in *Cxcr3*- and *Cx3cr1*-deficient mice or following FTY720 administration. These results suggest a role for this NK-cell subset in the control of tumor growth and are consistent with previous reports in which, using a transplantable model of LLC and a *Kras*-driven lung cancer model, CD27−CD11b+ mature NK cells were identified as the main NK-cell subset involved in lung tumor immune surveillance (50, 51). Of note, also in these experimental conditions, CXCR3 was found dispensable for the control of tumor growth (51).
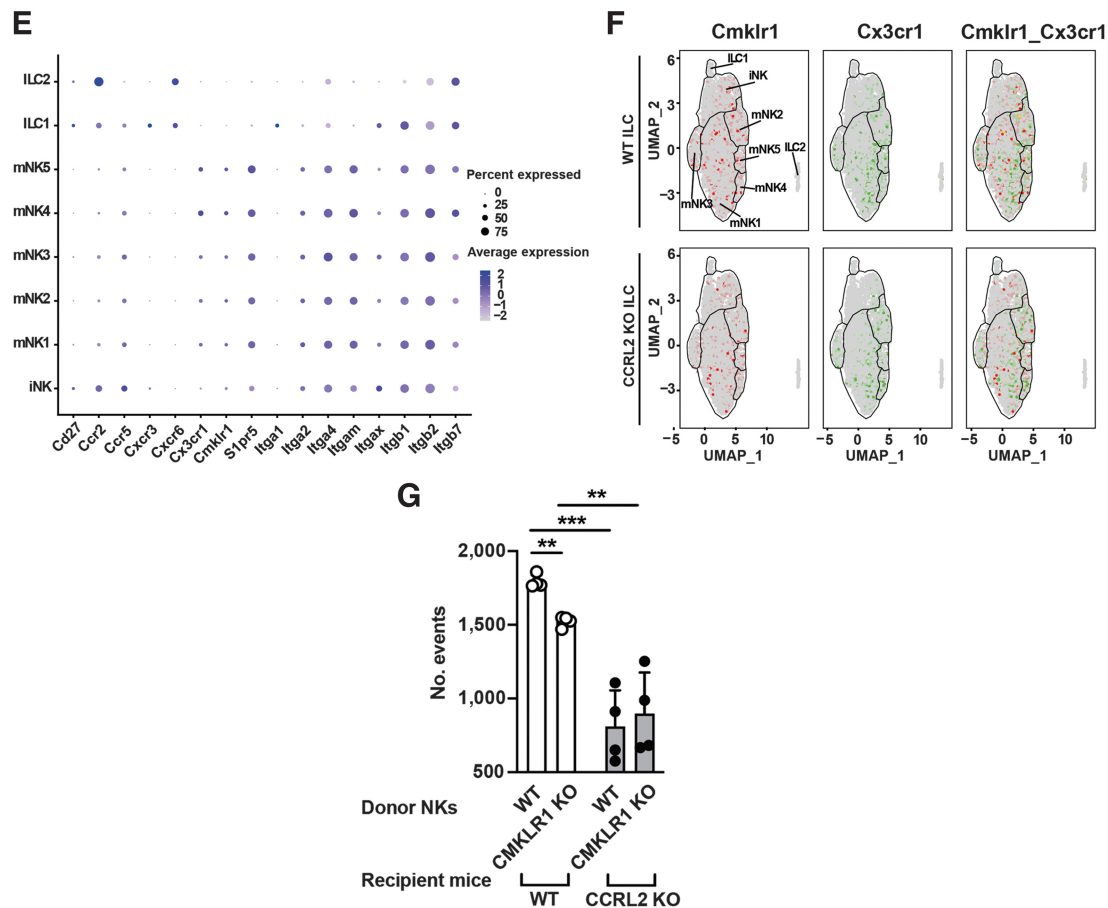

Figure 3.
CCRL2 marks specialized gCap lung endothelial cells as revealed by scRNA-seq analysis. **A,** UMAP of 47,491 lung *Pecam1* (CD31) positive cells from two published scRNA-seq datasets. Each different color in the graph highlights a specific cluster. **B,** Violin plots represented the distribution of lung endothelial gene expression programs defined in Gillich and colleagues (15), grouped by clusters. **C,** Violin plot represented the distribution of *Ccrl2* gene expression. Wilcoxon rank sum test and Bonferroni correction. ****, $P_{adj} < 0.0001$. **D,** Representative images of IF analysis of NKp46+ NK cells interacting with CD31+ lung endothelial cells in *Kras*$^{G12D/+}$; *p53*^{LoxP} TK WT and *Ccrl2*-deficient mice. Magnification, 40×. Right, quantification of the number of NK cells interacting with CD31+ lung endothelial cells evaluated on the entire sections evaluated. *, $P < 0.05$ TK WT tumors versus TK CCRL2 KO tumors by Student *t* test. **E,** Left, percentage of area occupied by tumor lesions on total lung area of *Cdh5*$^{Cre/ERT2}$;*Ccrl2*$^{f/f}$ versus *Ccrl2*$^{f/f}$ control mice intravenously injected with 10^5 KP10.21 cells and sacrificed 15 days later. **, $P < 0.01$, *Cdh5*$^{Cre/ERT2}$;*Ccrl2*$^{f/f}$ ($n = 6$) versus *Ccrl2*$^{f/f}$ mice ($n = 6$) by Student *t* test. Representative images of H&E staining of *Cdh5*$^{Cre/ERT2}$;*Ccrl2*$^{f/f}$, and *Ccrl2*$^{f/f}$ control lungs. Magnification, 10×. Right, flow cytometric analysis of NK cells in the CD45+ population from mechanically and enzymatically treated *Cdh5*$^{Cre/ERT2}$,*Ccrl2*$^{f/f}$, and *Ccrl2*$^{f/f}$ lungs. *, $P < 0.05$; *Cdh5*$^{Cre/ERT2}$; *Ccrl2*$^{f/f}$ ($n = 6$) versus *Ccrl2*$^{f/f}$ mice ($n = 6$) by Student *t* test. **F,** Violin plot represented the distribution of *Ackr2* expression in our murine lung scRNA-seq dataset. Wilcoxon rank sum test and Bonferroni correction. ****, $P_{adj} < 0.0001$. **G,** Percentage of area occupied by tumor lesions on total lung area of *Cdh5*$^{Cre/ERT2}$; *Ackr2*$^{f/f}$ versus *Ackr2*$^{f/f}$ control mice intravenously injected with 10^5 KP10.21 cells and sacrificed 15 days later. *Cdh5*$^{Cre/ERT2}$;*Ackr2*$^{f/f}$ ($n = 5$) versus *Ackr2*$^{f/f}$ ($n = 4$). Representative images of H&E staining of *Cdh5*$^{Cre/ERT2}$;*Ackr2*$^{f/f}$ and *Ackr2*$^{f/f}$ control lungs. Magnification, 10×. Right, flow cytometric analysis of NK cells in the CD45+ population from mechanically and enzymatically treated *Cdh5*$^{Cre/ERT2}$, *Ackr2*$^{f/f}$, and *Ackr2*$^{f/f}$ lungs.
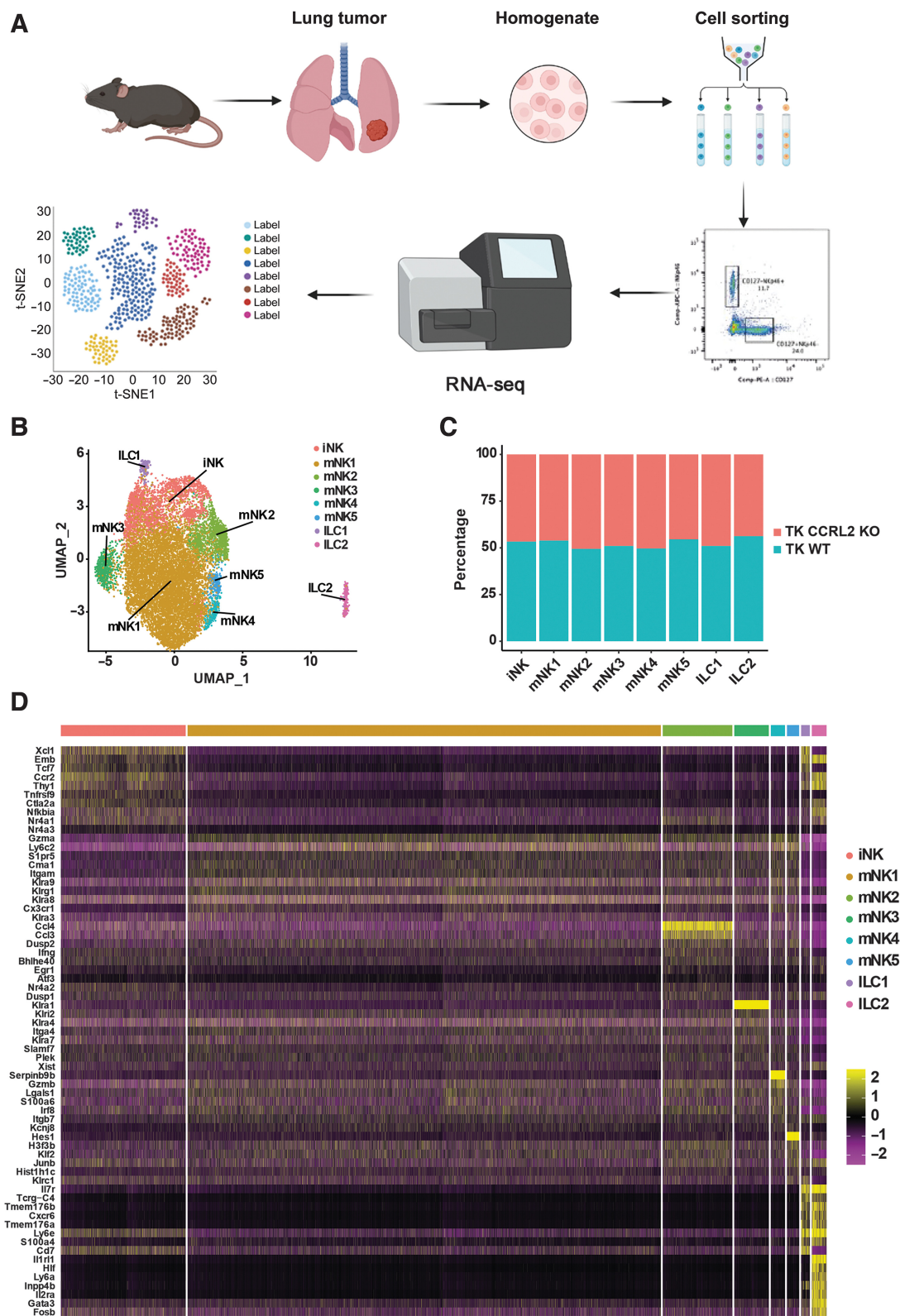
Figure 4.
scRNA-seq analysis of NK and ILC cells extracted from lung tumors of TK WT and TK *Ccrl2*-deficient mice. **A,** Workflow of scRNA-seq of sorted ILCs from mechanically and enzymatically treated TK WT and *Ccrl2* KO lungs. **B,** UMAP of 12,980 cells divided in 5,891 cells for the TK *Ccrl2*-deficient sample and 6,682 cells for the TK WT sample. Each different color in the legend highlights a specific cluster. **C,** Cellular distribution across each cluster, divided for genotype, is shown as stacked histogram. **D,** Heat map of the top 10 genes, tested with a Wilcoxon rank sum test, that better divided the cells into subsets. In yellow are highlighted overexpressed genes, in purple the downregulated ones. (*Continued on the following page.*)

Figure 4.
(*Continued.*) **E,** Dot-plot visualization of selected chemokine receptor and integrin genes. The size of dots represents the relative gene expression in percent for each cluster, while the blue color intensity indicates the average expression level for the indicated gene per cluster. **F,** Feature plots, for each genotype, showing single and double positive cells for *Cmklr1* and *Cx3cr1* genes in our NK scRNA-seq dataset. The expression of each gene was highlighted with a different color; cluster borders are shown with lines. **G,** Adoptive transfer of fluorescent labeled NK cells, purified from spleen of WT and *Cmklr1*-deficient mice, intravenously injected in tumor-bearing WT ($n = 4$) and *Ccrl2* deficient mice ($n = 4$) at day +14 after the injection of KP10.21 cells. After 24 hours, mice were sacrificed, and tumors harvested and processed for flow cytometric analysis. **, $P < 0.01$; ***, $P < 0.001$ by Student t test.

NK-cell maturation is characterized by the acquisition of different patterns of expression of chemotactic receptors. Mature NK cells mostly express CX3CR1, CMKLR1, and S1PR5 (13, 29, 52). This expression profile was confirmed by scRNA-seq of lung infiltrating NK cells (clusters mNK1–5) in our $Kras^{G12D/+};p53^{LoxP}$ tumor model. The same cell clusters were also characterized by the expression of integrin α chains (*Itga1, Itga2, Itgam,* and *Itga4*) and β chains (*Itgb1, Itgb2,* and *Itgb7*), which are required for migration into tissues. Despite the expression of multiple chemotactic receptors, our results support the distinctive requirement for CCRL2 in NK-cell migration to the lung for the control of tumor growth. This finding suggests a possible dual role for the CCRL2/chemerin/CMKLR1 axis in antitumor lung immune surveillance. A direct role in the recruitment of CMKLR1$^+$ NK cells and an accessory role in the proper localization of NK cells recruited by the action of different chemotactic factors. This model is supported by the evidence that a reduced frequency of *Cmklr1*$^+$ NK cells was found in the lung of *Ccrl2*-deficient mice and by the fact that most of the lung mature NK cells were found to coexpress *Cmklr1* and *Cx3cr1*. The possible existence of a cooperative role for CCRL2 with other chemotactic receptors is further suggested by the reduced migration to the

lung observed for both WT and *Cmklr1*-deficient NK cells when adoptively transferred into *Ccrl2*-deficient mice. It is also possible that the unique function of CCRL2 in lung immune surveillance may depend on the kinetics of action of different chemotactic factors, with the CCRL2/chemerin/CMKLR1 axis representing a ready-to-use chemotactic pathway and other chemotactic receptors being involved at later phases of tumor progression. It is worth noting that under physiologic conditions, chemerin is present in plasma at nanomolar concentrations as an immature inactive precursor that can be rapidly processed to the active form by the action of inflammation related proteases (7). In a *Kras*-driven lung cancer model, NK cells were shown to have an antitumor role in the early phases of tumor initiation but were dispensable at later stages of tumor promotion and progression. These results suggest CCRL2 as the predominant NK-cell chemotactic factor in the early phases of tumor immune surveillance preceding the action of other chemokines (50).

Lung alveolar capillary endothelial cells play a central role in the exchange of oxygen and carbon dioxide between air and blood (53) and represent the primary site of leukocyte trafficking to the lung (32). The mosaic organization of alveolar capillaries was recently elucidated at
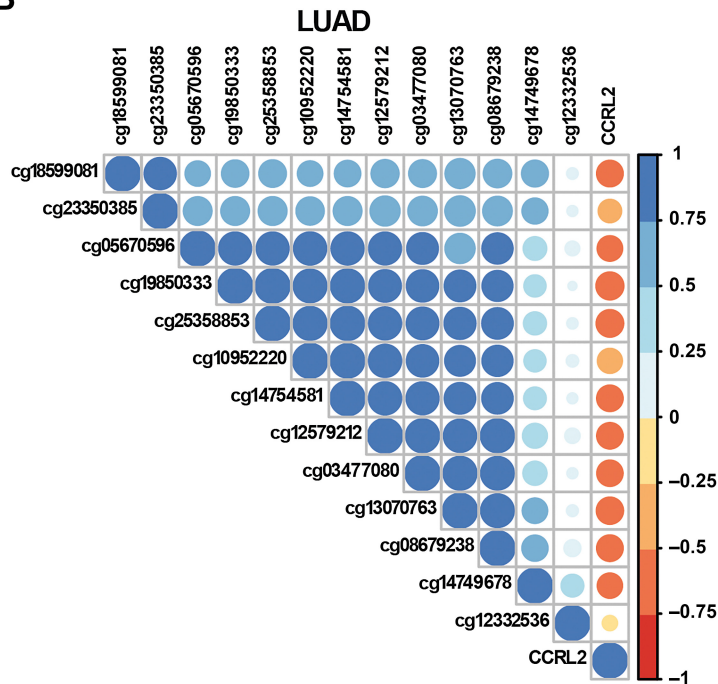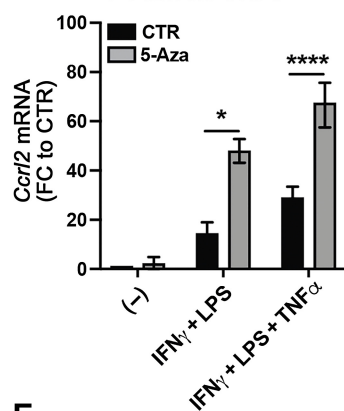
A LUAD CCRL2 expression

B LUAD
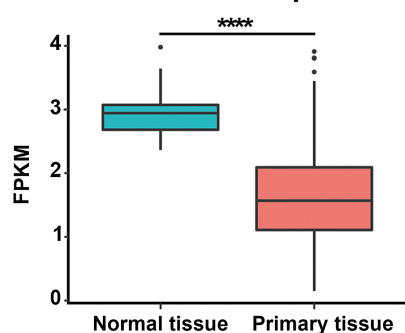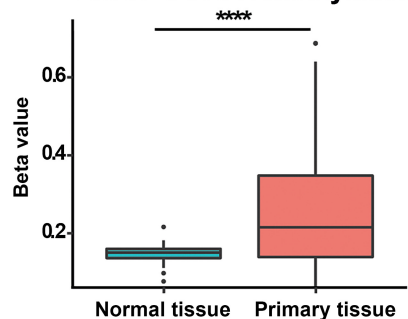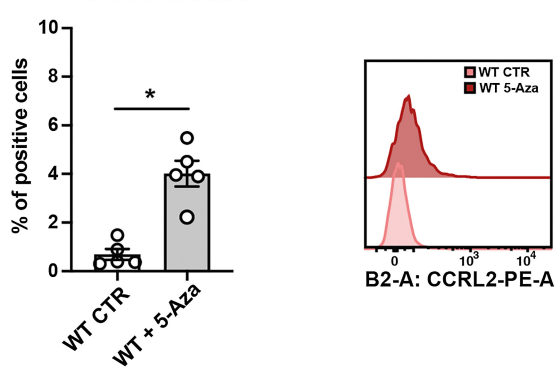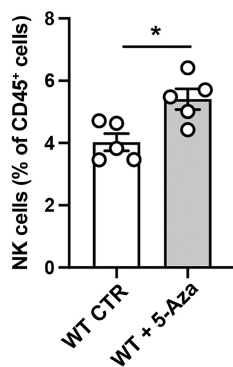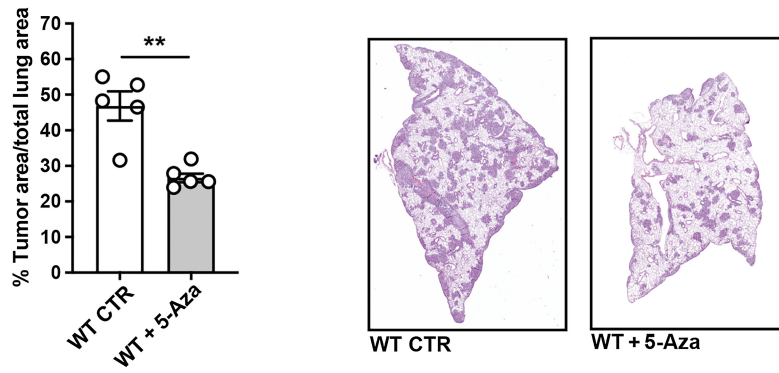
C 5-Aza *in vitro*

D CD31⁺CCRL2⁺

E

F 5-Aza *in vivo*

the single-cell level, showing that, similarly to the lung epithelial cell compartment, two major types of alveolar capillary endothelial cells exist, namely aerocytes (or aCaps), specialized in gas exchange, and general capillary cells (gCaps), specialized in the regulation of vaso-motor tone and endowed with functions of bipotent progenitor cells (15). Based on the transcriptional signature that includes adhe-sion molecules and chemokines, aCaps were proposed to represent the specialized site of leukocyte trafficking, whereas gCaps, expressing MHC class II components, were proposed to have a role in antigen presentation (15). However, genes encoding proteins involved in leukocyte recruitment, such as chemokines (e.g., CXCL12) and adhe-sion molecules (e.g., ICAM-1) are expressed also by gCaps. In addition, we show that both resting and activated gCaps express *Ccrl2*, which may promote in a chemerin-dependent manner the recruitment of cells expressing CMKLR1. Thus, our results suggest gCaps as an additional privileged site for leukocyte recruitment to the lung. aCaps express *Ctsl1*, a lysosomal cysteine protease that may participate in the cleavage of plasma prochemerin (54), fueling the CCRL2/chemerin/CMKLR1 chemotactic axis under both homeostatic and reactive conditions. Once activated, also aCaps may express *Ccrl2*, as observed in aCap clusters bearing the type I IFN gene signature. This suggests that under reactive conditions, aCaps may sustain a chemerin-dependent pathway for the recruitment of NK cells to the lung. Because gCaps can act as progenitor cells and differentiate into aCaps (15), it could be possible that CCRL2$^+$ aCaps carrying an IFN signature may originate from activated gCaps. However, pseudotemporal analysis did not support this hypothesis, suggesting the acquisition of a stable phenotype by these clusters. Activated aCaps and gCaps also express *Ackr2*. Similarly to CCRL2, ACKR2 does not activate G protein–dependent signaling or chemotaxis, but it possesses constitutive and ligand-stimulated scavenging activity, a process that contributes to control of the composition of the local proinflammatory microenvi-ronment (55, 56). Although it was recently proposed that ACKR2 may regulate the migration of NK cells to the lung (39), using mice carrying the selective deletion of *Ackr2* in the endothelial cell compartment (*Cdh5$^{Cre/ERT2}$;Ackr2$^{f/f}$* mice) we did not detect any alteration in NK-cell recruitment or lung tumor growth. Thus, this result excludes a direct role of ACKR2 expression by alveolar capillary endothelial cells in lung NK-cell immune surveillance.

CCRL2 is a nonsignaling seven transmembrane domain protein that binds the nonchemokine chemotactic factor chemerin (6, 7). We and others have previously reported that CCRL2 regulates *in vivo* multiple inflammatory pathologies, including hypersensitivity, arthritis, and sterile lung inflammation (10, 11, 17, 18, 57, 58). One of the proposed mechanisms of action of this molecule is based on the expression of CCRL2 by endothelial cells, where it acts as a presenting molecule. By binding chemerin, CCRL2 can form a membrane gradient active in the recruitment of circulating cells that express CMKLR1, the functional chemerin receptor. We have previously reported that CMKLR1 is expressed by different leukocyte subsets, including antigen-presenting cells (APC; ref. 14) and NK cells (13). Here we provide genetic evidence

that demonstrates the relevance of this mechanism for the recruitment of NK cells *in vivo*. In addition, we show that *in vivo*, CCRL2 is selectively expressed by lung alveolar capillary endothelial cells. Because plasma prochemerin can be processed by proteases expressed by endothelial cells, including aCaps, to generate the active form, we propose that the CCRL2/chemerin/CMKLR1 axis may represent a selective pathway for the recruitment of NK cells to the lung. The selective expression of CCRL2 by alveolar capillary endothelial cells here reported in the mouse is apparently conserved also in humans, making this finding of potential clinical relevance. The unique expres-sion of CCRL2 by lung endothelium also explains why CCRL2 plays a protective role in lung tumors, but it does not protect from tumors growing in different tissues, such as subcutaneous tumors.

This study also shows that CCRL2 is epigenetically regulated in endothelial cells *in vitro* and *in vivo* and that the administration of hypomethylating agents may promote the localization of effector immune cells to the lung. This aspect is worth of further investigation in the context of combined anticancer therapies to increase targeting of NK cells or chimeric antigen receptor NK (CAR-NK) cells to the lung (59).

The discovery and characterization of members of the chemo-kine family has provided understanding of the mechanisms govern-ing the selective homing of leukocyte subsets to specific organs (1, 60, 61). In the past few years, this concept has begun to be exploited for adaptive immune cells, such as T and B cells, with more limited effort in the definition of homing signals for innate cells. On the basis of the results here presented, we propose the CCRL2/chemerin/CMKLR1 axis as a new pathway for the homing of NK cells to the lung.

Authors' Disclosures

Authors' Contributions

F. Sozio: Investigation and methodology. **T. Schioppa:** Investigation and methodology. **M. Laffranchi:** Formal analysis and validation. **V. Salvi:** Investiga-tion and methodology. **N. Tamassia:** Formal analysis. **F.M. Bianchetto-Aguilera:** Formal analysis. **L. Tiberio:** Investigation and methodology. **R. Bonecchi:** Formal

Figure 5.
CCRL2 expression is epigenetically regulated on lung endothelial cells. **A,** Distribution of *CCRL2* expression values (top) reported as FPKM, both for tumor and normal tissues. *CCRL2* methylation values (bottom) were presented as βvalues, both for tumor and normal tissues. Data were derived from the TCGA LUAD dataset. Student *t* test (****, *P* < 0.0001). **B,** Correlation plot in the tumoral sample showed in **A,** between *CCRL2* expression and its methylation state assessed by the indicated probes. In blue are shown positive correlations, vice versa in red are labeled the negative correlations. **C,** *Ccrl2* expression on 5-Aza–treated or untreated mouse lung capillary endothelial cell line 1G11 unstimulated or stimulated with proinflammatory stimuli (IFNγ, LPS, TNF). FC is indicated. *, *P* < 0.05; ****, *P* < 0.0001 5-Aza–treated versus untreated 1G11 cells by one-way ANOVA and Bonferroni correction. **D,** Flow cytometric analysis (% of positive cells and MFI) of CCRL2$^+$CD31$^+$ cells in lungs of PBS (CTR) and 5-Aza–treated tumor-bearing WT mice. *, *P* < 0.05 by Student *t* test, WT CTR (*n* = 5) versus 5-Aza–treated WT mice (*n* = 5). **E,** Flow cytometric analysis of NK cells in the CD45$^+$ population from mechanically and enzymatically treated tumor-bearing WT CTR and 5-Aza–treated WT mice. *, *P* < 0.05, CTR versus 5-Aza–treated WT mice. **F,** Tumor burden of CTR and 5-Aza–treated WT mice. **, *P* < 0.01 CTR versus 5-Aza–treated WT mice by Student *t* test. Representative images of H&E staining. Magnification, 10×.

Acknowledgments

Note

Supplementary data for this article are available at Cancer Immunology Research Online (http://cancerimmunolres.aacrjournals.org/).

References

1. Griffith JW, Sokol CL, Luster AD. Chemokines and chemokine receptors: positioning cells for host defense and immunity. Annu Rev Immunol 2014; 32:659–702.
2. Mantovani A, Allavena P, Sozzani S, Vecchi A, Locati M, Sica A. Chemokines in the recruitment and shaping of the leukocyte infiltrate of tumors. Semin Cancer Biol 2004;14:155–60.
3. Zabel BA, Rott A, Butcher EC. Leukocyte chemoattractant receptors in human disease pathogenesis. Annu Rev Pathol 2015;10:51–81.
4. Graham GJ, Handel TM, Proudfoot AEI. Leukocyte adhesion: reconceptualizing chemokine presentation by glycosaminoglycans. Trends Immunol 2019;40:472–81.
5. Bachelerie F, Graham GJ, Locati M, Mantovani A, Murphy PM, Nibbs R, et al. New nomenclature for atypical chemokine receptors. Nat Immunol 2014;15: 207–8.
6. Zabel BA, Nakae S, Zúñiga L, Kim JY, Ohyama T, Alt C, et al. Mast cell-expressed orphan receptor CCRL2 binds chemerin and is required for optimal induction of IgE-mediated passive cutaneous anaphylaxis. J Exp Med 2008;205:2207–20.
7. Bondue B, Wittamer V, Parmentier M. Chemerin and its receptors in leukocyte trafficking, inflammation and metabolism. Cytokine Growth Factor Rev 2011; 22:331–8.
8. De Henau O, Degroot GN, Imbault V, Robert V, De Poorter C, Mcheik S, et al. Signaling properties of chemerin receptors CMKLR1, GPR1 and CCRL2. PLoS One 2016;11:e0164179.
9. Mazzotti C, Gagliostro V, Bosisio D, Del Prete A, Tiberio L, Thelen M, et al. The atypical receptor CCRL2 (C-C chemokine receptor-like 2) does not act as a decoy receptor in endothelial cells. Front Immunol 2017;8:1233.
10. Monnier J, Lewén S, O'Hara E, Huang K, Tu H, Butcher EC, et al. Expression, regulation, and function of atypical chemerin receptor CCRL2 on endothelial cells. J Immunol 2012;189:956–67.
11. Gonzalvo-Feo S, Del Prete A, Pruenster M, Salvi V, Wang L, Sironi M, et al. Endothelial cell-derived chemerin promotes dendritic cell transmigration. J Immunol 2014;192:2366–73.
12. Kennedy AJ, Davenport AP. International union of basic and clinical pharmacology CIII: chemerin receptors CMKLR1 (Chemerin. Pharmacol Rev 2018;70: 174–96.
13. Parolini S, Santoro A, Marcenaro E, Luini W, Massardi L, Facchetti F, et al. The role of chemerin in the colocalization of NK and dendritic cell subsets into inflamed tissues. Blood 2007;109:3625–32.
14. Wittamer V, Franssen JD, Vulcano M, Mirjolet JF, Poul EL, Migeotte I, et al. Specific recruitment of antigen-presenting cells by chemerin, a novel processed ligand from human inflammatory fluids. J Exp Med 2003;198:977–85.
15. Gillich A, Zhang F, Farmer CG, Travaglini KJ, Tan SY, Gu M, et al. Capillary cell-type specialization in the alveolus. Nature 2020;586:785–9.
16. Kalucka J, de Rooij LPMH, Goveia J, Rohlenova K, Dumas SJ, Meta E, et al. Single-cell transcriptome atlas of murine endothelial cells. Cell 2020;180: 764–79.
17. Del Prete A, Sozio F, Schioppa T, Ponzetta A, Vermi W, Calza S. et al. The atypical receptor CCRL2 is essential for lung cancer immune surveillance. Cancer Immunol Res 2019;7:1775–88.
18. Otero K, Vecchi A, Hirsch E, Kearley J, Vermi W, Del Prete A, et al. Nonredundant role of CCRL2 in lung dendritic cell trafficking. Blood 2010;116:2942–9.
19. Cossarizza A, Chang HD, Radbruch A, Acs A., Adam D, Adam-Klages S, et al. Guidelines for the use of flow cytometry and cell sorting in immunological studies (second edition). Eur J Immunol 49:1457–973 2019.
20. Hao Y, Hao S, Andersen-Nissen E, Mauck WM, Zheng S, Butler A, et al. Integrated analysis of multimodal single-cell data. Cell 2021;184:3573–87.
21. Stuart T, Butler A, Hoffman P, Hafemeister C, Papalexi E, Mauck WM. et al. Comprehensive integration of single-cell data. Cell 2019;177:1888–902.
22. Hafemeister C, Satija R. Normalization and variance stabilization of single-cell RNA-seq data using regularized negative binomial regression. Genome Biol 2019;20:296.
23. Robinette ML, Fuchs A, Cortez VS, Lee JS, Wang Y, Durum SK, et al. Transcriptional programs define molecular characteristics of innate lymphoid cell classes and subsets. Nat Immunol 2015;16:306–17.
24. Tabula Muris Consortium. Single-cell transcriptomics of 20 mouse organs creates a tabula muris. Nature 2018;562:367–72.
25. Cao J, Spielmann M, Qiu X, Huang X, Ibrahim DM, Hill AJ, et al. The single-cell transcriptional landscape of mammalian organogenesis. Nature 2019;566:496–502.
26. Raudvere U, Kolberg L, Kuzmin I, Arak T, Adler P, Peterson H, et al. g:Profiler: a web server for functional enrichment analysis and conversions of gene lists (2019 update). Nucleic Acids Res 2019;47:W191–8.
27. DuPage M, Dooley AL, Jacks T. Conditional mouse lung cancer models using adenoviral or lentiviral delivery of Cre recombinase. Nat Protoc 2009; 4:1064–72.
28. Al Delbany D, Robert V, Dubois-Vedrenne I, Del Prete A, Vernimmen M, Radi A, et al. Expression of CCRL2 inhibits tumor growth by concentrating chemerin and inhibiting neoangiogenesis. Cancers (Basel) 2021;13:5000.
29. Walzer T, Vivier E. G-protein-coupled receptors in control of natural killer cell migration. Trends Immunol 2011;32:486–92.
30. Russo E, Laffranchi M, Tomaipitinca L, Del Prete A, Santoni A, Sozzani S, et al. NK cell anti-tumor surveillance in a myeloid cell-shaped environment. Front Immunol 2021;12:787116.
31. Lämmermann T, Kastenmüller W. Concepts of GPCR-controlled navigation in the immune system. Immunol Rev 2019;289:205–31.
32. Lien DC, Wagner WW, Capen RL, Haslett C, Hanson WL, Hofmeister SE, et al. Physiological neutrophil sequestration in the lung: visual evidence for localization in capillaries. J Appl Physiol (1985) 1987;62;1236–43.
33. Negretti NM, Plosa EJ, Benjamin JT, Schuler BA, Habermann AC, Jetter CS, et al. A single-cell atlas of mouse lung development. Development 2021;148:dev199512.
34. Schuler BA, Habermann AC, Plosa EJ, Taylor CJ, Jetter C, Negretti NM, et al. Age-determined expression of priming protease TMPRSS2 and localization of SARS-CoV-2 in lung epithelium. J Clin Invest 2021;131:e140766.
35. Travaglini KJ, Nabhan AN, Penland L, Sinha R, Gillich A, Sit RV, et al. A molecular cell atlas of the human lung from single-cell RNA sequencing. Nature 2020;587:619–25.
36. Jones RC, Karkanias J, Krasnow MA, Pisco AO, Quake SR, Salzman J, et al. The tabula sapiens: a multiple-organ, single-cell transcriptomic atlas of humans. Science 2022;376:eabl4896.

37. Kadur Lakshminarasimha Murthy P, Sontake V, Tata A, Kobayashi Y, Macadlo L, Okuda K, et al. Human distal lung maps and lineage hierarchies reveal a bipotent progenitor. Nature 2022;604:111–9.

38. Mantovani A, Bonecchi R, Locati M. Tuning inflammation and immunity by chemokine sequestration: decoys and more. Nat Rev Immunol 2006;6:907–18.

39. Hansell CAH, Fraser AR, Hayes AJ, Pingen M, Burt CL, Lee KM, et al. The atypical chemokine receptor Ackr2 constrains NK cell migratory activity and promotes metastasis. J Immunol 2018;201:2510–9.

40. Crinier A, Milpied P, Escalière B, Piperoglou C, Galluso J, Balsamo A, et al. High-dimensional single-cell analysis identifies organ-specific signatures and conserved NK cell subsets in humans and mice. Immunity 2018;49:971–86.

41. Mindt BC, Fritz JH, Duerr CU. Group 2 innate lymphoid cells in pulmonary immunity and tissue homeostasis. Front Immunol 2018;9:840.

42. Meininger I, Carrasco A, Rao A, Soini T, Kokkinou E, Mjösberg J. Tissue-specific features of innate lymphoid cells. Trends Immunol 2020;41:902–17.

43. Crinier A, Kerdiles Y, Vienne M, Cózar B, Vivier E, Berruyer C. Multidimensional molecular controls defining NK/ILC1 identity in cancers. Semin Immunol 2021;52:101424.

44. Bjaanæs MM, Fleischer T, Halvorsen AR, Daunay A, Busato F, Solberg S, et al. Genome-wide DNA methylation analyses in lung adenocarcinomas: association with EGFR, KRAS and TP53 mutation status, gene expression and prognosis. Mol Oncol 2016;10:330–43.

45. Serin I, Dogu MH. The use of hypomethylating agents in hematologic malignancies: treatment preferences and results. Int J Hematol Oncol 2021;10:IJH37.

46. Momparler RL. Epigenetic therapy of non-small cell lung cancer using decitabine (5-aza-2'-deoxycytidine). Front Oncol 2013;3:188.

47. Wang L, Amoozgar Z, Huang J, Saleh MH, Xing D, Orsulic S, et al. Decitabine enhances lymphocyte migration and function and synergizes with CTLA-4 blockade in a murine ovarian cancer model. Cancer Immunol Res 2015;3:1030–41.

48. Xiao X, Xu Q, Sun Y, Lu Z, Li R, Wang X, et al. 5-aza-2'-deoxycytidine promotes migration of acute monocytic leukemia cells via activation of CCL2-CCR2-ERK signaling pathway. Mol Med Rep 2017;16:1417–24.

49. Wendt MK, Johanesen PA, Kang-Decker N, Binion DG, Shah V, Dwinell MB. Silencing of epithelial CXCL12 expression by DNA hypermethylation promotes colonic carcinoma metastasis. Oncogene 2006;25:4986–97.

50. Cong J, Wang X, Zheng X, Wang D, Fu B, Sun R, et al. Dysfunction of natural killer cells by FBP1-induced inhibition of glycolysis during lung cancer progression. Cell Metab 2018;28:243–55.

51. Yamamoto Y, Miyazato K, Takahashi K, Yoshimura N, Tahara H, Hayakawa Y. Lung-resident natural killer cells control pulmonary tumor growth in mice. Cancer Sci 2018;109:2670–6.

52. Sciumè G, De Angelis G, Benigni G, Ponzetta A, Morrone S, Santoni A, et al. CX3CR1 expression defines 2 KLRG1+ mouse NK-cell subsets with distinct functional properties and positioning in the bone marrow. Blood 2011;117:4467–75.

53. Hsia CC, Hyde DM, Weibel ER. Lung structure and the intrinsic challenges of gas exchange. Compr Physiol 2016;6:827–95.

54. Kulig P, Kantyka T, Zabel BA, Banas M, Chyra A, Stefanska A, et al. Regulation of chemerin chemoattractant and antibacterial activity by human cysteine cathepsins. J Immunol 2011;187:1403–10.

55. Bonecchi R, Graham GJ. Atypical chemokine receptors and their roles in the resolution of the inflammatory response. Front Immunol 2016;7:224.

56. Graham GJ, Locati M. Regulation of the immune and inflammatory responses by the 'atypical' chemokine receptor D6. J Pathol 2013;229:168–75.

57. Schioppa T, Sozio F, Barbazza I, Scutera S, Bosisio D, Sozzani S, et al. Molecular basis for CCRL2 regulation of leukocyte migration. Front Cell Dev Biol 2020;8:615031.

58. Del Prete A, Martínez-Muñoz L, Mazzon C, Toffali L, Sozio F, Za L, et al. The atypical receptor CCRL2 is required for CXCR2-dependent neutrophil recruitment and tissue damage. Blood 2017;130:1223–34.

59. Xie G, Dong H, Liang Y, Ham JD, Rizwan R, Chen J. CAR-NK cells: a promising cellular immunotherapy for cancer. EBioMedicine 2020;59:102975.

60. Butcher EC. Leukocyte-endothelial cell recognition: three (or more) steps to specificity and diversity. Cell 1991;67:1033–6.

61. Springer TA. Traffic signals for lymphocyte recirculation and leukocyte emigration: the multistep paradigm. Cell 1994;76:301–14.